Intercomparison of Multi-Day Simulations of Convection during TOGA COARE with Several Cloud-Resolving and Single-Column Models

S. K. Krueger and S. M. Lazarus
Department of Meteorology
University of Utah
Salt Lake City, Utah

Introduction

The goal of the Global Energy and Water Experiment (GEWEX) Cloud System Study (GCSS) is to improve the parameterization of cloud-related processes in global climate models (GCMs) through an improved physical understanding of these processes. The main tool of GCSS is the cloud-resolving model (CRM), which is a numerical model that resolves cloud-scale (and mesoscale) circulations in either two or three spatial dimensions. In contrast, a GCM cannot resolve the individual convective cells or even the accompanying mesoscale circulations. Therefore, the collective effects of these sub-grid scale processes must be parameterized. A CRM is able to determine these collective effects directly, to the extent that its representation of grid-scale dynamics and the parameterizations of its own sub-grid processes are accurate. A general approach for using CRMs, in conjunction with single-column models (SCMs) and observations, to test and develop parameterizations for GCMs was described by Randall et al. (1996).

GCSS Working Group 4 (WG 4, Precipitating Convective Cloud Systems) recently completed two projects designed to evaluate CRMs and SCMs using Tropical Ocean Global Atmosphere-Coupled Ocean Atmosphere Response Experiment (TOGA-COARE) data sets (Moncrieff et al. 1997). This paper describes one of these projects (Case 2). For additional information, see Krueger (1997a, b) or the WG 4 website (http://www.met.utah.edu/skrueger/gcss/wg4.html).

Case 2 evaluated CRMs and SCMs by testing their ability to determine the large-scale (domain and time-averaged) statistics of precipitating convective cloud systems during a multi-day period. We selected a 6-day period from December 20 to 26, 1992, which included several episodes of deep convection. The large-scale quantities required for the simulations (initial conditions, upper and lower boundary conditions, and large-scale forcing) are based on observations averaged over the Intensive Flux Array (IFA, about 500 km by 500 km). The participating models included seven two-dimensional (2-D) CRMs, one three-dimensional (3-D) CRM, and nine SCMs (see Table 1). The

Table 1. Models and modelers that participated in the Case 2 intercomparison.

Model	Modeler(s)
1-D SCMs	
Bechtold:	
Betts-Miller	P. Bechtold
Kain-Fritsch	P. Bechtold
Tiedtke	P. Bechtold
Tiedtke-Nordeng	P. Bechtold
No convection	P. Bechtold
Community Climate Model, Version 3 (CCM3)	J. Petch
Colorado State University (CSU)	D. Cripe D. Randall
European Centre for Medium-range Weather Forecasting (ECMWF)	D. Gregory
United Kingdom Meteorological Office (UKMO)	J. Cairns
2-D CRMs	
Centre National de Recherches Météorologiques (CNRM)	F. Guichard, J.-L. Redelsperger
CSU	K.-M. Xu
Goddard Cumulus Ensemble (GCE) Model	D. Johnson W.-K. Tao
Geophysical Fluid Dynamics Laboratory (GFDL)	C. Seaman L. Donner
National Center for Atmospheric Research (NCAR)	X. Wu W. Grabowski
Regional Atmospheric Modeling System (RAMS)	H. Jiang R. McAnelly
University of Utah (UU)	S. Krueger
3-D CRMs	
NCAR/PSU Mesoscale Model 5 (UW MM5)	H. Su S. Chen

models have been evaluated by comparing the results of the simulations to observed large-scale (IFA-averaged) quantities (see Table 2).

Model Evaluation

We expect differences between the CRM and SCM simulations and the observations to occur due to 1) use of a 2-D geometry (for 2-D CRM simulations); 2) use of a small domain (for 3-D CRM simulations); 3) uncertainties in the microphysics, radiation, and turbulence parameterizations; 4) uncertainties in the parameterizations of cloud amount and cumulus convection (for SCM simulations); 5) specifying the large-scale advective tendencies of hydrometers as zero; 6) errors in the observational estimates of the large-scale advective tendencies of potential temperature and water vapor; and 7) limitations of the observations used to evaluate the simulations.

Table 2. TOGA-COARE IFA observations used for model evaluation.

Quantity	Source
Temperature profile	rawinsondes[1]
Water vapor profile	rawinsondes[1]
Cloud cover	International Satellite Cloud Climatology Program (ISCCP)[2]
"Cloud top" temperature	ISCCP[2]
"Cold" cloud cover	ISCCP[2]
Liquid water path (LWP) + ice water path (IWP)	ISCCP optical depth[2]
IWP	Special Sensor Microwave (SSM)/T-2[3]
Cloud water profile	---
Cloud ice profile	---
Cloud fraction profile	rawinsondes[4]
Radiative fluxes:	
Surface downwelling solar	IMET buoy, 2 ships, 2 islands[5]; FC[6]
Surface downwelling infrared (IR)	IMET buoy, 2 ships, 2 islands[5]; FC[6]
Top of the atmosphere (TOA) upwelling solar	ISCCP Flux Cloud (FC)[6], Geostationary Meteorological Satellite (GMS)-Collins[7], GMS-Minnis[8]
TOA upwelling IR	ISCCP FC[6], GMS-Collins[7], GMS-Minnis[8]
Surface turbulent fluxes	IMET and Tropical Atmosphere Ocean (TAO) buoys[9]

(1) Lin and Johnson (1996a)
(2) Rossow and Schiffer (1991)
(3) Liu and Curry (1998)
(4) Wang et al. (1998)
(5) Krueger and Burks (1998)
(6) Zhang et al. (1995); Rossow and Zhang (1995)
(7) Collins et al. (1997)
(8) Doelling et al. (1998)
(9) Lin and Johnson (1996b)

We will present two examples of evaluation of model results: one based on outgoing longwave radiation (OLR) measurements, and the second on cloud water path (CWP) estimates. Figure 1 shows the time series of the OLR for the CRMs and the SCMs, along with the IFA observations. The observed OLR has minima near 24, 72, and 120 hours. (The time coordinate in Figures 1 and 2 are relative to 00 UTC December 20, 1992.) The OLR minima are associated with extensive high cloudiness over the IFA. Satellite imagery shows that during the first 3 days, much of the cloudiness formed outside the IFA and was advected into it, while during the last 3 days (hours 72 to 144), nearly all of the cloudiness formed and dissipated within the IFA.

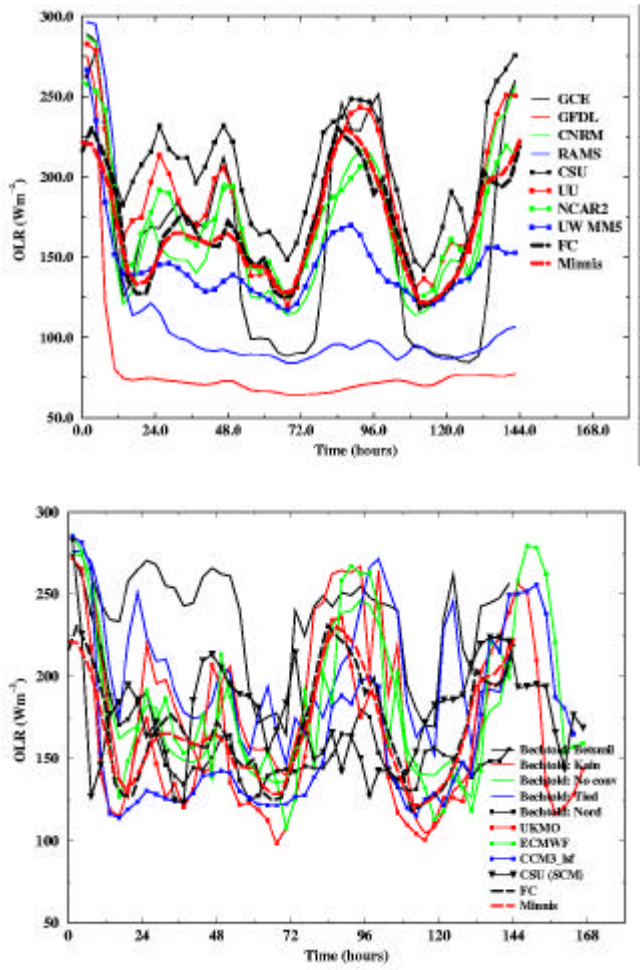

Figure 1. Time series of the OLR for the CRMs (top) and the SCMs (bottom), along with the IFA observations (FC, Minnis). (For a color version of this figure, please see *http://www.arm.gov/docs/documents/technical/conf_9803/krueger(2)-98.pdf*.)

Measurements of hydrometer advection into the IFA were not available, so the large-scale advective tendencies of hydrometers were set to zero in the simulations. As a result, when using models with realistic representations of cloud formation and dissipation, we would expect noticeable differences between the simulated and the observed cloud fields during periods in which significant hydrometer advection occurred (i.e., during the first 3 days), and smaller differences during periods in which hydrometer advection was insignificant (i.e., during the last 3 days). We also expect, in general, that the representation of cloud processes is more realistic in CRMs than in SCMs. The time series of the OLR for the CRMs (Figure 1, top panel) is consistent with our expectations: except for GFDL, RAMS, UW MM5, and to a lesser extent GCE, the OLR time series are generally larger than observed during the first 3 days, while they are close to observed during the last 3 days. In contrast, the OLR time series for the SCMs (Figure 1, bottom panel), while generally correlated with the observations, exhibit more high-frequency variability that is uncorrelated with the observations.

Figure 2 shows time series of the CWP for the CRMs and the SCMs, along with the IFA observations. The CWP observations are estimates based on the ISCCP retrievals of visible optical depth τ. The ISCCP optical depth retrieval assumes that clouds consist of water droplets and that the effective radius, τ_e, of the droplets is 10 microns. Then

$$\mathrm{CWP} = \frac{2}{3}\tau\rho_L\tau_e,$$

where ρ_L is the is the density of water. The ISCCP optical depths during the night are interpolated values.

The CWP time series for the CRMs and the SCMs differ notably in their degree of correlation with the observations, as did their OLR time series. Because the CRM results in general are in much better agreement with the OLR and CWP observations than are the SCM results, the CRM results should be useful for improving the SCMs. Systematic differences between the SCM and CRM results were identified for several other quantities, as well.

The similarities between the results from the CRMs and the observations for OLR and CWP, among others, confirms that the bulk characteristics of convection are determined (in a diagnostic sense) by the large-scale thermodynamic advective tendencies, and suggests that CRMs are useful tools for performing this diagnosis. Additional CRM results

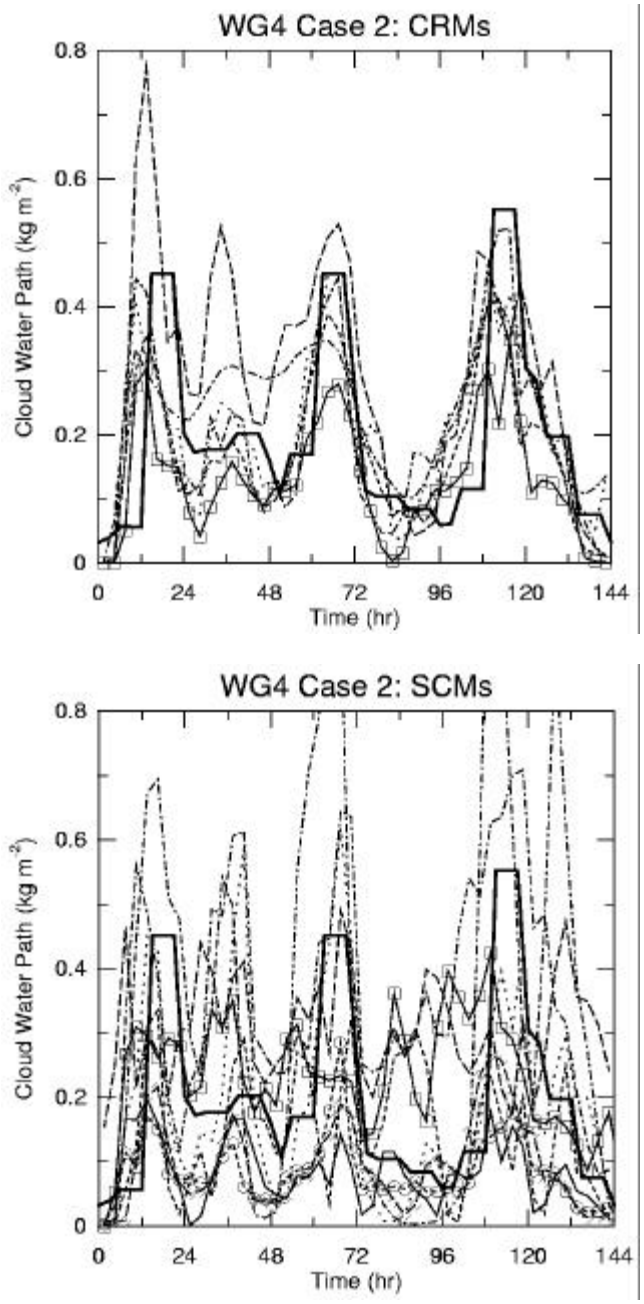

Figure 2. Time series of the CWP (cloud water path) for the CRMs (top) and the SCMs (bottom), along with the IFA observations (heavy solid line).

indicate that the IWP, the cloud fraction, and the TOA radiative fluxes due to deep tropical cumulus convection are basically parameterizable in terms of the cloud mass flux (Krueger 1997a, b; Xu and Krueger 1991).

Temperature Errors and the Large-Scale Forcing

Figure 3 shows the profiles of the temperature error (difference between simulated and observed temperature), averaged over the last 5 days of the 6-day simulations, for the CRMs and the SCMs. All simulations averaged 2 K to 3 K colder than observed below 12 km. The CRM profiles are remarkably similar to one another (except for GFDL and RAMS), as are the SCM profiles (except for "Bechtold: No conv," which did not include a cumulus parameterization, and CSU above 6 km). The time variations of the CRM temperature errors are also highly correlated (Krueger 1997a, b). These features suggest that the temperature errors have a common origin external to the models: errors in the imposed large-scale advective tendencies of potential temperature and/or water vapor.

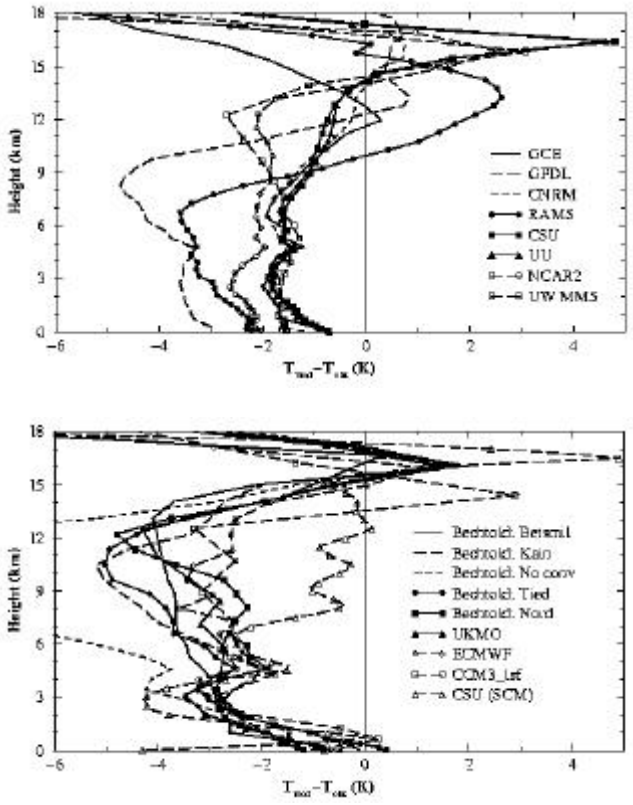

Figure 3. Profiles of the 5-day average temperature error (difference between simulated and observed temperature) for the CRMs (top) and the SCMs (bottom).

We have checked this conjecture by careful analysis of the budget of IFA-averaged tropospheric moist static energy (TMSE). Although it would seem more appropriate to examine the budget of tropospheric potential temperature (or that of a closely related quantity, dry static energy), the budget of TMSE is a better choice because it does not involve phase changes (i.e., net condensation). Consequently, analysis of the observed budget does not require knowledge of the surface rainfall rate, which is difficult to measure accurately, and the budget for a simulation does not depend on the representation of moist convection, which varies from model to model (Emanuel and Zivkovic-Rothman 1998).

Moist static energy is

$$h \equiv c_p T + Lq + gz,$$

where c_p is the specific heat of air at constant pressure, T is the air temperature, L is the latent heat of condensation, q is the water vapor mixing ratio, g is gravity, and z is the height. The budget of TMSE is

$$\frac{\partial[\bar{h}]}{\partial t} = \left(\frac{\partial[\bar{h}]}{\partial t}\right)_{L.S.} + \left(\bar{\rho}\overline{w'h'}\right)_0 + \left[\overline{Q_R}\right],$$

where an overbar indicates an average over the IFA and brackets indicate a mass-weighted average over the troposphere. The budget equation consists of the tendency of TMSE, the forcing of TMSE by large-scale advection, the forcing of TMSE by turbulent surface fluxes, and the forcing of TMSE by radiative heating, respectively. The forcing of TMSE by net melting of hydrometers is neglected because it is small compared to the other terms.

This budget equation is obeyed by the CRMs and SCMs. In the Case 2 simulations, the prescribed large-scale advective forcing of TMSE is based upon the analysis by Lin and Johnson (1996a), while the remaining TMSE forcing terms are predicted by the models themselves. In all simulations, the TMSE averaged over the last 5 days is less than observed. The TMSE errors are directly related to the temperature errors and could be due to errors in any of the three TMSE forcing terms. However, the model predictions for the forcing terms are generally quite similar to the observed values (Burks 1998). This suggests that the TMSE errors in the Case 2 simulations are due to the imposed large-scale advective forcing.

The above conclusions are based on only 5 days out of the 4-month COARE Intensive Observation Period (IOP). We also used observational estimates of the TMSE tendency and the TMSE forcing components for the entire 4-month COARE IOP to calculate the budget residual, or imbalance. We used an analysis by Ciesielski (1996; available from http://kiwi.atmos.colostate.edu/scm/toga-coare.html) that is very similar to Lin and Johnson's (1996a) analysis to calculate the tendency and the large-scale advective forcing of TMSE during the COARE IOP. Figure 4 shows the time series of the observed tendency (top) and the forcing by large-scale advection (bottom), each averaged over 5-day periods for the entire IOP.

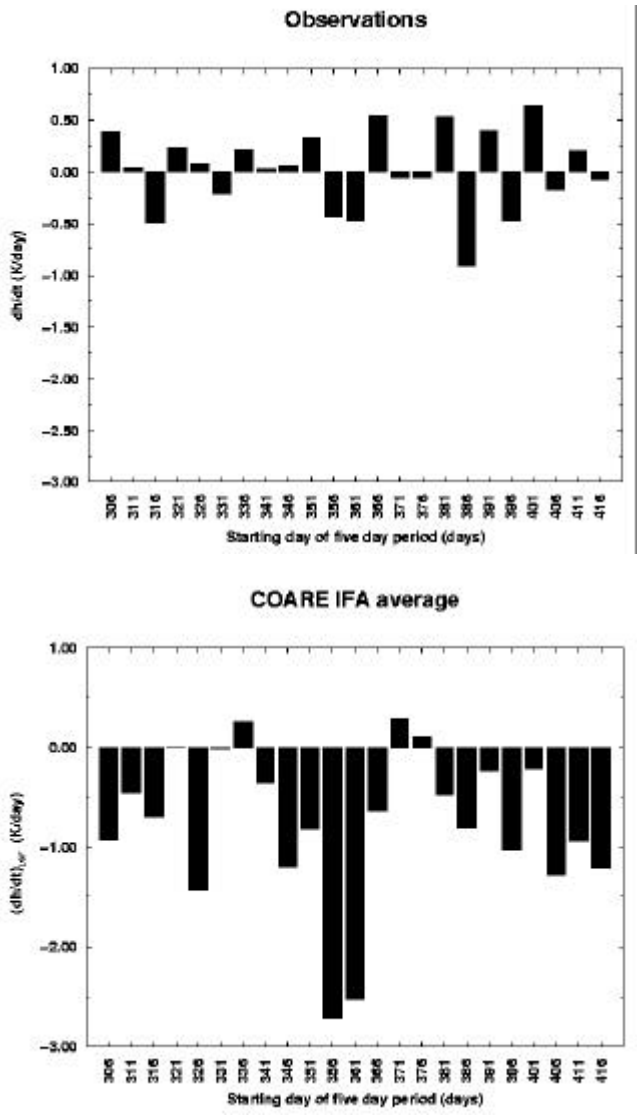

Figure 4. Time series of the IFA-averaged tropospheric moist static energy budget components: the observed tendency (top) and forcing by large-scale advection (bottom), each averaged over 5-day periods for the COARE IOP.

The forcing by turbulent surface fluxes is based upon Lin and Johnson's (1996b) analysis. We used three observational estimates for the radiative forcing: FC, Minnis (5 station), and Collins (5 station). These are based on the IFA-averaged radiative flux estimates at the surface and TOA listed in Table 2 and described by Burks (1998) and Krueger and Burks (1998). Figure 5 shows the time series of the forcing by turbulent surface fluxes (top) and the forcing by radiative heating (bottom), each averaged over 5-day periods for the entire IOP.

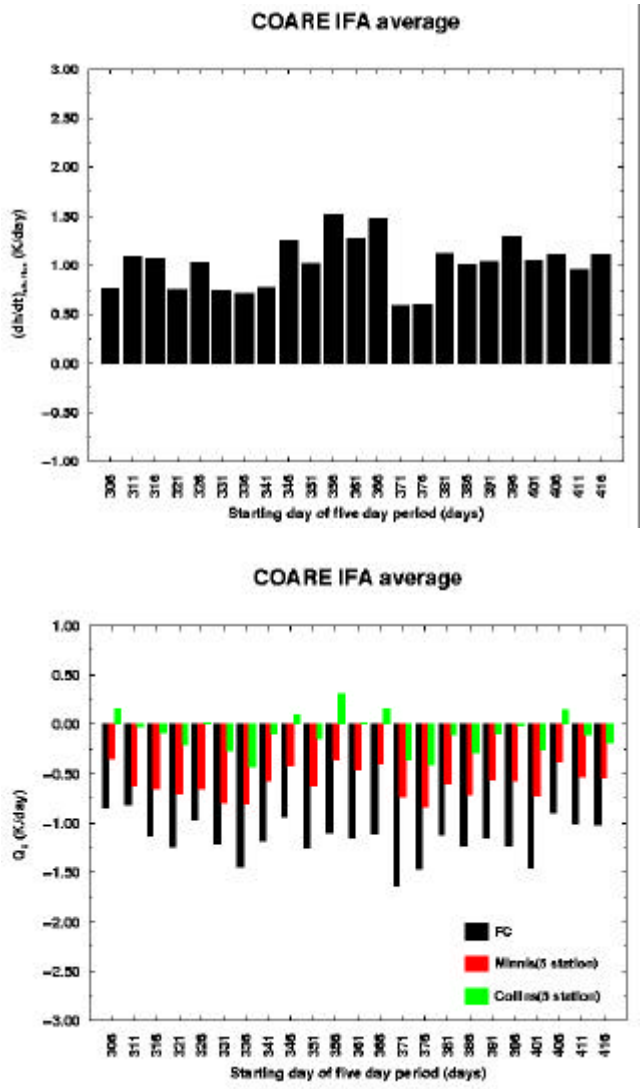

Figure 5. Time series of the IFA-averaged tropospheric moist static energy budget components: forcing by turbulent surface fluxes (top) and forcing by radiative heating (bottom), each averaged over 5-day periods for the COARE IOP. (For a color version of this figure, please see *http://www.arm.gov/docs/documents/technical/conf_9803/krueger(2)-98.pdf*.)

The TMSE budget imbalance is the tendency implied by the observational estimates of the forcing components (i.e., the sum of the forcing components) minus the observed tendency. Figure 6 shows the time series of the budget imbalance averaged over 5-day periods for the entire IOP.

The uncertainty of the TMSE tendency estimates is about 0.1 K/day, as is the uncertainty of the turbulent surface flux forcing estimates, while the uncertainty of the radiative heating estimates (as suggested by the differences between the three data sets) is about 0.5 K/day. Figure 6 shows that regardless of the choice of radiative heating data set used, the budget is not balanced (within the remaining uncertainty of about 0.2 K/day) for all 5-day periods. This leads us to conclude, as before, that the budget imbalance is due to errors in the large-scale advective forcing.

It should be noted that it is unlikely that the TMSE budget equation will be satisfied by independent observational analyses of each budget term. However, a new integrated analysis technique has been developed by Zhang (1998) that includes such budget constraints. Zhang plans to use his technique to analyze the large-scale advective forcing over the IFA for the COARE IOP.

Figure 6 also shows that the budget imbalance for the Case 2 period (starting day 356) is the largest of the entire IOP. The budget imbalance for the Case 2 period ranges from -0.75 K/day to -2.25 K/day, with a mean of -1.5 K/day.

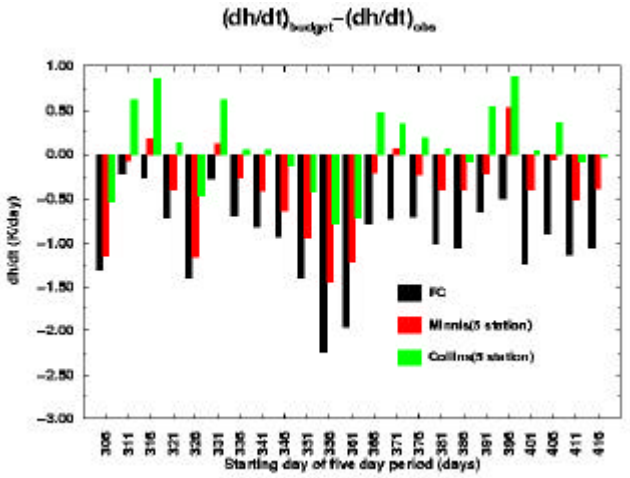

Figure 6. Time series of the IFA-averaged tropospheric moist static energy budget imbalance (sum of forcing components minus the observed tendency) averaged over 5-day periods for the COARE IOP. (For a color version of this figure, please see *http://www.arm.gov/docs/documents/technical/conf_9803/krueger(2)-98.pdf*.)

Over 2.5 days, the mean imbalance would produce a TMSE error of -3.75 K. This is somewhat larger than the simulation errors because there was a tendency in the simulations to counteract the cooling.

Acknowledgments

This research was supported by the Environmental Science Division, U.S. Department of Energy (DOE), under Grant DE-FG03-94ER61769.

References

Burks, J. E., 1998: Radiative fluxes and heating rates during TOGA COARE over the intensive flux array. M.S. thesis, Department of Meteorology, University of Utah, Salt Lake City, 85 pp.

Collins, W. D., A. Bucholtz, and F. P. Valero, 1997: Derivation of top of atmosphere fluxes from geostationary satellites using high altitude aircraft measurements: Results from COARE and CEPEX. Preprints, *9th Conference on Atmospheric Radiation*, Amer. Meteo. Soc., 198-202.

Doelling, D. R., P. Minnis, R. Palikonda, and D. Spangenberg, 1998: Validation of broadband fluxes derived from GMS during TOGA COARE. *Proceedings, CLIVAR/GEWEX COARE98 Conference*, Boulder, Colorado, WCRP, in press.

Emanuel, K., and M. Zivkovic-Rothman, 1998: Development and evaluation of a convection scheme for use in climate models. *J. Atmos. Sci*., accepted.

Krueger, S. K., 1997a: A GCSS intercomparison of cloud-resolving models based on TOGA COARE observations. *Proceedings of the ECMWF/GCSS Workshop on New Insights and Approaches to Convective Parameterization*, Reading, England, U.K., ECMWF, 113-127.

Krueger, S. K., 1997b: Intercomparison of multi-day simulations of convection during TOGA COARE with several cloud-resolving models. *Preprints, 22nd Conference on Hurricanes and Tropical Meteorology*, Fort Collins, Colorado, Amer. Meteor. Soc., 63-64.

Krueger, S. K., and J. E. Burks, 1998: Radiative fluxes and heating rates during TOGA COARE over the intensive flux array. This proceedings.

Lin, X., and R. H. Johnson, 1996a: Kinematic and thermodynamic characteristics of flow over the western Pacific warm pool during TOGA COARE. *J. Atmos. Sci*., **53**, 695-715.

Lin, X., and R. H. Johnson, 1996b: Heating, moistening, and rainfall over the western Pacific warm pool during TOGA COARE. *J. Atmos. Sci*., **53**, 3367-3383.

Liu, G., and J. Curry 1998: Tropical cloud ice water amount and its relation to other cloud properties as determined by satellite and aircraft microwave measurements. *Proceedings of the CLIVAR/GEWEX COARE98 Conference*, Boulder, Colorado, WCRP, in press.

Moncrieff, M. W., S. K. Krueger, D. Gregory, J.-L. Redelsperger, and W.-K. Tao, 1997: GEWEX Cloud System Study (GCSS) Working Group 4: Precipitating convective cloud systems. *Bull. Amer. Met. Soc*., **78**, 831-845.

Randall, D. A., K.-M. Xu, R. J. C. Somerville, and S. Iacobellis, 1996: Single-column models and cloud ensemble models as links between observations and climate models. *J. Climate*, **9**, 1683-1697.

Rossow, W. B., and R. A. Schiffer, 1991: ISCCP cloud data products. *Bull. Amer. Meteor. Soc*., **71**, 2-20.

Rossow, W. B., and Y.-C. Zhang, 1995: Calculation of surface and top-of-atmosphere radiative fluxes from physical quantities based on ISCCP data sets: 2. Validation and first results. J. *Geophys. Res*., **100**, 1167-1197.

Wang, J., J. Curry, and W. Rossow, 1998: Cloud vertical structure in TOGA-COARE, *Proceedings, CLIVAR/ GEWEX COARE98 Conference*, Boulder, Colorado, WCRP, in press.

Xu, K.-M., and S. K. Krueger, 1991: Evaluation of cloudiness parameterizations using a cumulus ensemble model. *Mon. Wea. Rev*., **119**, 342-367.

Zhang, M. H., 1998: Integrating ARM measurements to force and evaluate GCM parameterizations. This proceedings.

Zhang, Y.-C., W. B. Rossow, and A. A. Lacis, 1995: Calculation of surface and top-of-atmosphere radiative fluxes from physical quantities based on ISCCP data sets: 1. Method and sensitivity to input data uncertainties. *J. Geophys. Res*., **100**, 1149-1165.